



# Thermo-mechanical analysis of a micro-engineered tungsten-foam armored IFE FW

M. Andersen\*, S. Sharafat, N. Ghoniem

*University of California Los Angeles, 420 Westwood Plaza, Los Angeles, CA 90095-1597, USA*

Received 31 January 2005; received in revised form 27 September 2005; accepted 27 September 2005  
Available online 27 December 2005

## Abstract

The high average power laser (HAPL) program goal is to develop a laser inertial fusion reactor using a solid first wall (FW). The FW of the inertial fusion energy (IFE) chamber is exposed to high energy photon, particle, and neutron fluxes at frequency of several Hz. The feasibility of using a micro-engineered refractory metals, such as tungsten foam as a solid FW armor is investigated. Refractory foams are a new class of materials with very limited thermo-mechanical property databases. Elastic properties of tungsten foams are not readily available, particularly at high temperatures. To estimate high-temperature elastic properties of tungsten foams, a three-dimensional finite-element model of tungsten foam was developed. True stress strain curves of tungsten foams at elevated temperatures were developed as a function of characteristic foam properties and compared with measured values. The thermo-mechanical response of the tungsten-foam armored FW was analyzed using a detailed three-dimensional finite element model. The thermo-mechanical response of a tungsten-foam protected first wall to a typical IFE pulse is presented. It is shown that the W foam armor can be tailored to meet the thermo-mechanical stress requirements of an IFE solid wall design.

© 2005 Published by Elsevier B.V.

*Keywords:* Metallic foam; Inertial confinement; Armor; First wall; High heat load

## 1. Introduction

The high average power laser (HAPL) program is a coordinated effort to develop laser inertial fusion energy [1]. The HAPL program is pursuing the development of a solid first wall (FW) chamber. A solid

dry FW must be designed to withstand the effects of repetitive bursts of X-rays, ions, and neutrons assumed unimpeded by any gas in the chamber. X-rays and ions have shallow penetration depths of 0.5 and 1–5  $\mu\text{m}$ , respectively [2–5]. Although, X-rays (1%) and ions (27%) account for only a small portion of the total load, they cause the most damage because that load is dispersed over such a small volume [6]. Shallow energy absorption leads to fast expansion in the surface while the bulk prevents the expansion [3,4]. This high sur-

\* Corresponding author. Tel.: +1 310 825 8917;  
fax: +1 310 206 4830.

*E-mail address:* [manders2129@aol.com](mailto:manders2129@aol.com) (M. Andersen).

face stress leads to numerous deformation phenomena such as roughening, wrinkling, permanent plasticity, cracking, etc. In addition, the high intensity energy can lead to near instantaneous melting, evaporation, and plasma formation. The armor must be in a form such that the spread of energy would be quasi-volumetric and would allow for structural flexibility. A porous material, such as foam, presents the opportunity to control both depth of energy deposition, and the mode of deformation.

However, the heterogeneous geometry of the foam structures poses a challenge for thermo-mechanical analysis, in particular using finite element modeling (FEM). The foam cannot be modeled as a homogeneous material with volume-averaged foam material properties. Instead, a detailed three-dimensional model of the foam structure needs to be created. For IFE conditions volume averaged material properties resulted in erroneous results, such as complete melting of the tungsten foam, which contradicts experimental findings [11]. Here we present the results of a detailed three-dimensional finite element modeling effort to analyze the thermo-mechanical response of a tungsten-foam armored FW exposed to IFE radiation conditions.

## 2. Micro-engineered tungsten armor

The X-rays provide the highest heating power of  $7.91 \times 10^{18} \text{ W/m}^3$ , which only lasts 1 ns and penetrates  $\sim 0.5 \mu\text{m}$  into the surface under the HAPL target spectrum [6]. The neutrons on the other hand have a much longer mean free path. A volumetric power

deposition of  $8.2 \times 10^{14} \text{ W/m}^3$  is experienced by a  $5 \mu\text{m}$  thick tungsten FW armor followed by deposition of  $2.3 \times 10^{14} \text{ W/m}^3$  to the underlying 3 mm steel structure. The neutron flux only lasts 10 ns and will have a more damaging affect on the long term as opposed to a pulse-by-pulse basis. The most damaging heating comes from the helium ions, because they expose the wall for nearly  $4 \mu\text{s}$  to power levels as high as  $1.76 \times 10^{16} \text{ W/m}^3$ . First wall radiation and heating loading history used in the FEM analysis are summarized in Table 1.

Refractory foams are a new class of open-cell foams that are used for a variety of aerospace and industrial applications ranging from thermal insulation to impact absorbers [7–10]. For a more detailed discussion of IFE relevant refractory foam applications the reader is referred to earlier publications [11,12]. Metallic foams can be engineered starting with polymer foams, which are first converted to reticulated vitreous carbon (RVC) foams. The RVC foam is further processed using chemical vapor infiltration (CVI), to produce ceramic or metal foams [13]. The materials can be simultaneously optimized for stiffness, strength, thermal conductivity, active surface area, and gas permeability. Among the materials that can be deposited are the refractory metals (e.g. niobium, tantalum, tungsten, and rhenium) and their ceramic compounds.

The most common cell structure of foams is the tetrakaidecahedron unit cell. It contains 14 faces, has 36 edges, and 24 vertices. The interconnecting ligaments provide an enormous surface area per unit volume, called geometric surface area. In 80–100 pores per inch (ppi) densities, the surface area varies from 12.3 to  $1.76 \times 10^4 \text{ m}^2/\text{m}(\text{solid})^3$  [14].

Table 1  
Single pulse load history on the FW of a 6.5-m radius HAPL IFE chamber used for FEM conditions for ANSYS modeling [6]

Source	Start (s)	End (s)	Duration (s)	Depth (m)	Load ( $\text{W/m}^3$ )
X-rays	0	$1.0 \times 10^{-9}$	$1.0 \times 10^{-9}$	$0.5 \times 10^{-6}$	$7.91 \times 10^{18}$
No load	$1.0 \times 10^{-9}$	$90.0 \times 10^{-9}$	$89.0 \times 10^{-9}$		0
Neutrons (shallow)	$90.0 \times 10^{-9}$	$100.0 \times 10^{-9}$	$10.0 \times 10^{-9}$	$5.0 \times 10^{-6}$	$8.2 \times 10^{14}$
Neutrons (deep)				$3.0 \times 10^{-3}$	$2.3 \times 10^{14}$
No load	$100.0 \times 10^{-9}$	$2.0 \times 10^{-7}$	$2.0 \times 10^{-7}$		0
Burn ions	$2.0 \times 10^{-7}$	$2.8 \times 10^{-7}$	$0.8 \times 10^{-7}$	$5.0 \times 10^{-6}$	$8.7 \times 10^{15}$
No load	$2.8 \times 10^{-7}$	$1.0 \times 10^{-6}$			0
Debris ions	$1.0 \times 10^{-6}$	$3.75 \times 10^{-6}$	$2.75 \times 10^{-6}$	$1.0 \times 10^{-6}$	$1.76 \times 10^{16}$
No load	$3.75 \times 10^{-6}$	0.2	0.2		0

### 3. Transient thermal analysis

The foam protects the underlying FW steel structure from IFE X-rays and  $\alpha$ -particles. However, the foam must not insulate the underlying FW structure. To ensure that the W-foam will withstand IFE operating conditions the following must be investigated: (1) temperature profile throughout the foam during the pulse to assure that temperatures do not exceed melting; (2) check the boundary between the W-foam and steel for any high temperature occurrences that may damage the braze; (3) demonstrate that the foam's porous nature acts as a "thermal shock absorber" with quasi-volumetric energy absorption.

A three-dimensional CAD solid model of a segment of tungsten-foam armor attached to a ferritic FW was constructed and then analyzed using the FEM program ANSYS. The ligaments in this model were modeled to be uniform with square cross sections. Initial sizing for the ligaments were set at  $80\ \mu\text{m} \times 20\ \mu\text{m} \times 20\ \mu\text{m}$  corresponding to a porosity of 100 ppi (pore per inch). The foam matrix is attached to a FW steel structure in such a way to avoid any direct line of sight through the foam to the underlying steel. The meshed structure representing the tungsten-foam armor is shown in Fig. 1.

Results of the transient thermal analysis of the W-foam during one pulse are presented in Fig. 2. At

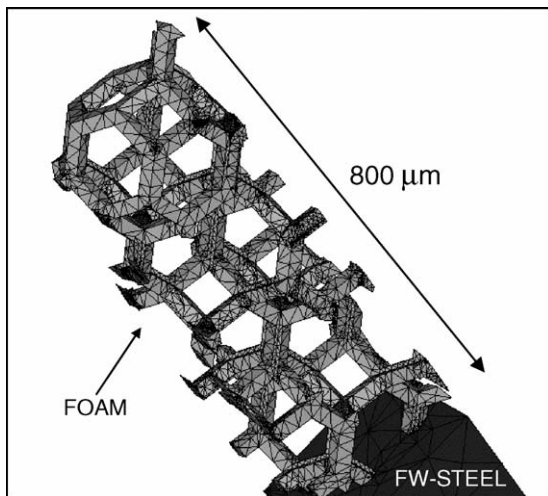


Fig. 1. Meshed finite element model of tungsten-foam armor (0.8 mm) protected ferritic steel first wall (3 mm).

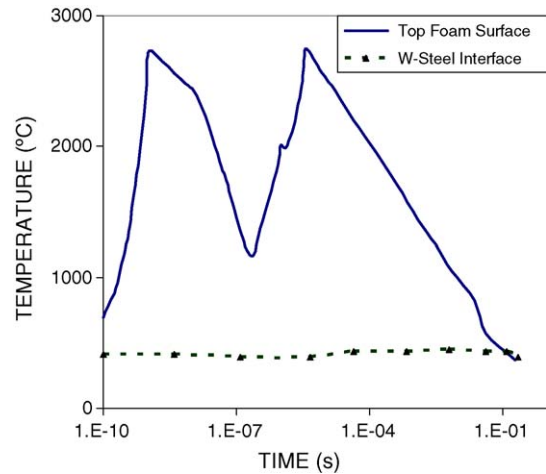


Fig. 2. Temperature profiles of the top tungsten-foam ligament surface and the foam/FW-steel interface throughout single heat pulse.

1 ns, X-rays heat the foam causing the first temperature spike. The foam then cools until the microsecond range at which time ions deposit their energy in the ligaments and raise the temperature before cooling back to near the initial average temperature of  $400\ ^\circ\text{C}$  within about 0.1 s. The steel heats to no more than  $500\ ^\circ\text{C}$ , which is well below the maximum allowable for FW ferritic steels. The maximum temperature takes place over a small area surrounding the contact between foam and steel and is quickly dissipated proving that thermal protection of the first wall can be facilitated by using a thin layer ( $\sim 0.25\ \text{mm}$ ) of tungsten-foam armor. The W-foam successfully protects the steel from melting because it acts as a heat dispersion structure that absorbs the heat over a large volume. The many surfaces and porous nature allow the entire volume of the foam to be used in such a way that ligaments near the steel handle only a portion of the load, enabling the upper levels to manage the bulk of heating. This is accomplished because less and less area of the foam is in line-of-sight deeper into the foam. Therefore, the smaller the loaded surface the smaller the resulting heat flux and hence the cooler the ligaments will be.

The temperatures at the upper (plasma side) and lower (steel facing) surfaces of selected ligaments are shown in Fig. 3 for four different depths in the foam starting with the top (plasma facing) ligament and ending with the ligaments that are in contact with the steel. The nodes selected represent the hot spots for each

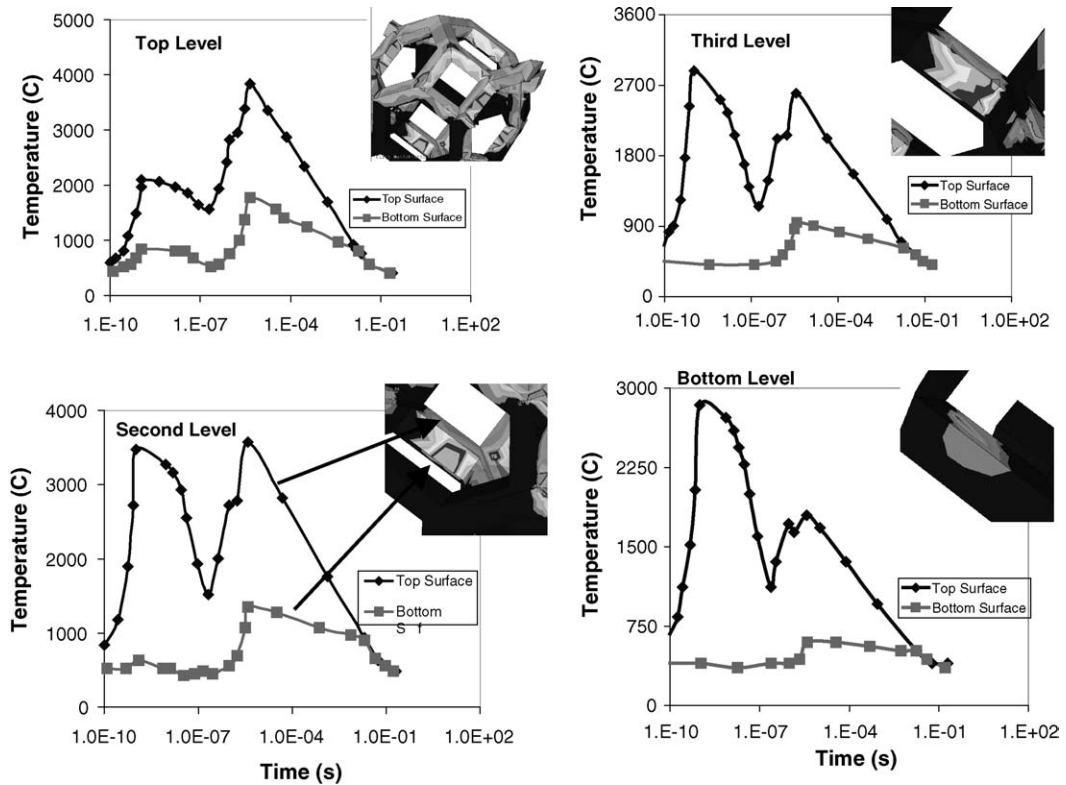


Fig. 3. Upper and lower foam ligament surface temperature evolution at four levels of the foam during one entire heat pulse (top level:  $x = 0 \mu\text{m}$ ; second level:  $x = 200 \mu\text{m}$ ; third level:  $x = 400 \mu\text{m}$ ; bottom level:  $x = 600 \mu\text{m}$  from the plasma facing side).

surface. Generally, the upper surfaces of the ligaments experience the same temperature excursion. They have a similar temperature pattern except for the lowest layer of ligaments, which had the smallest heated areas. The X-rays have little effect on the bottom temperatures of the ligaments, because of the shallow deposition depth ( $\sim 0.5 \mu\text{m}$ ) and short deposition time ( $\sim 1 \text{ ns}$ ). At a depth of only  $3 \mu\text{m}$ , the X-ray effect is negligible. The ions on the other hand are able to affect the lower ligament surface temperatures throughout all levels of the foam because of their long deposition time. This effect diminishes on deeper levels of the foam, but can still be observed at the bottom, if only slightly.

#### 4. Thermal stress analysis

The temperatures from the transient analysis along with high temperature true stress strain data for tung-

sten [12] were used to study the elasto-plastic response of the tungsten-foam armor. The foam framework effectively absorbs transient thermal stresses by bending and twisting of ligaments. The maximum thermal stress was about 1.5 GPa, which was caused by the localized high temperature along  $90^\circ$  sharp edges of the model. The foam experienced no plastic strain and reaches a maximum stress of about 100 MPa at the foam–steel interface during each heating cycle.

#### 5. Stress–strain behavior of foam

The heterogeneous morphology of foam structures results in characteristic stress strain behavior, which depends on foam geometry parameters such as, foam density, pore density, cell architecture, ligament thickness and length, and hollow or solid ligaments. This multi-parameter dependency necessitates experimental

measurements to obtain foam performance curves. An attempt is made here to develop the stress–strain curve for hollow ligament tungsten foam with a Kelvin cell geometry having a 100 ppi pore density, a relative density of 21%, and ligament dimensions of 80  $\mu\text{m}$  long and 20  $\mu\text{m}$  thick. The FEM results are compared with measured stress–strain curves.

A second FEM model of the tungsten foam with the same geometry of 64 cells was developed using pipe elements that allows for bending, rotation, and stretching while incorporating a hollow interior. The Kelvin cell geometry was modeled and non-linear tungsten properties were used. Stress–strain curves were generated by constraining one side of the foam and displacing the opposite in a normal direction away from the fixed side. The strains were based on the amount of deformation as compared to the original foam height. The stress was determined from the summation of forces at constrained points and cross-sectional area including porosity. The analysis was run at 30 and 1750  $^{\circ}\text{C}$ . Fig. 4 shows the derived stress–strain curves. The low temperature (30  $^{\circ}\text{C}$ ) analysis indicates that the foam experiences two-stress peaks followed by stress relaxation before complete failure. At higher temperatures

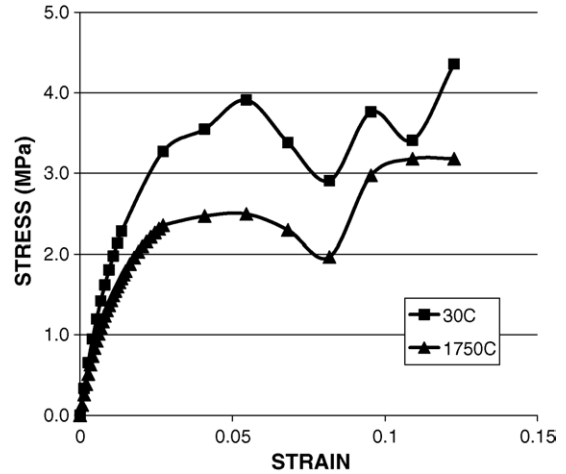


Fig. 4. FEM derived stress–strain curves for 100 ppi and 21% dense tungsten foam at two temperatures using low-strain high temperature stress–strain data [16] of polycrystalline tungsten.

(1750  $^{\circ}\text{C}$ ) the yield stress as well as the elastic modulus decrease and the foam undergoes only one stress relief cycle before failure. The stress at which yielding begins drops from about 2.5 MPa at 30  $^{\circ}\text{C}$  to about

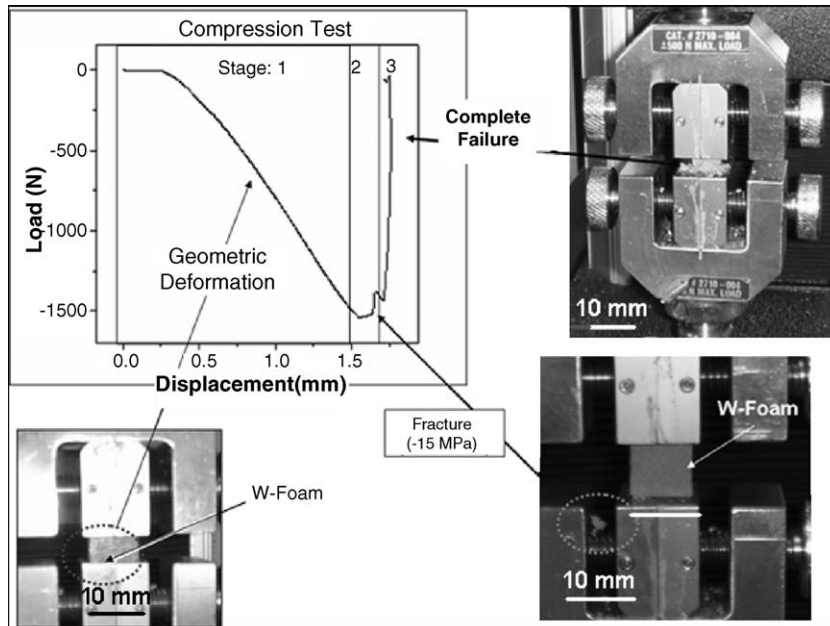


Fig. 5. Compression test of cubic centimeter 100 ppi and 21% dense tungsten foam showing three stages of response: (1) geometric deformation; (2) onset of fracture; (3) complete failure.

1.5 MPa at 1750 °C. Once yielding begins, the stresses remain roughly constant over a range of 5–10% displacement and then begin to increase again for both temperatures. This takes place because of the geometric hardening effect. The greatest stresses occur in the interior of the foam on ligaments most parallel to the line of displacement. The maximum stress for a strain of 0.0164 was found to be about 1.2 GPa, with an average of around 700 MPa. These isolated regions of high stress should play an important role because they will be the first to fracture resulting in stress relief.

Compression tests were performed on several 100 ppi and 21% dense W-foam samples supplied by Ultramet [15]. The volumetric fraction of the foam was 17% tungsten on a 4% TaC ligament skeleton (ligament core). The samples were cut into 1 cm × 1 cm × 1 cm cubes and compressed to failure using an INSTRON 5544. The rate of compression ranged from 0.05 to 0.5 mm/min. The testing revealed three stages of foam deformation, similar to the three stages derived for the low temperature FEM model shown in Fig. 4. Fig. 5 shows depictions of general foam behavior under the testing. As the foam is initially compressed, the sides bulge and the foam becomes more round as the stress is increased. This is followed by internal cracking where portions of the foam may break away from the edges accompanied by snapping sounds. The cracking relieves stress as the deformation continues. The final step is complete failure when the foam completely shatters or breaks into two large pieces along a diagonal crack. This is signified by a complete drop in the stress.

## 6. Conclusions

A fundamental concern of a solid FW in an IFE reactor is the long term thermo-mechanical survivability of the FW against the effects of high temperature pulsed operation. Micro-engineered materials, such as tungsten refractory foams are suggested as a first wall armor material to address these fundamental concerns. The open cell structure of foams transforms the high surface loads into “quasi-volumetric” heating. Tungsten foams with pore densities of 100 ppi have been manufactured and were investigated as potential FW armor material.

Thermal analysis indicates that a ferritic FW is well protected from high temperature excursions by employing thin tungsten-foam armor. Thermo-mechanical analysis shows that thermal stresses can be reacted by the rotation and deformation of the foam ligaments. Compression tests of 100 ppi tungsten foam with relative density of 21% were also performed and it was shown that the predicted failure stress was in good agreement with the measured values.

Although, significant challenges remain tungsten-foam materials are shown to constitute a potential candidate FW armor materials for IFE reactors.

## Acknowledgments

The authors would like to thank the High Average Power Laser program, which is sponsored by the Naval Research Laboratories for the opportunity and continued support of this work.

## References

- [1] J.D. Sethian, M. Friedman, R.H. Lehmburg, M. Myers, S.P. Obenschain, J. Giuliani, et al., Fusion energy with lasers, direct drive targets, and dry wall chambers, *Nucl. Fusion* 43 (2003) 1693–1709.
- [2] N. Ghoniem, Kulcinski, A critical assessment of the effects of pulsed irradiation on the microstructure, swelling, and creep of materials, *Nucl. Technol. Fusion* 2 (2) (1982) 165–198.
- [3] A. El-Azab, N. Ghoniem, Mechanical response and fatigue analysis of the first wall structure of the prometheus ife reactor, *Fusion Eng. Des.* 27 (1995) 536–543.
- [4] E.G. Lovell, R. Peterson, R. Engelstad, G. Moses, Transient elastic stresses in icf reactor first wall structural systems, in: UWFDM-421, Also The Second Topical Meeting on Fusion Reactor Materials, Seattle, WA, 1981.
- [5] J. Latkowski, Issues and activities for issues and activities for laser-ife optics, Snowmass, CO., July 10, 2002.
- [6] J. Blanchard, Threat spectra for HAPL targets, in: HAPL Meeting at Naval Research Laboratories, Washington, D.C., December 2–3, 2002.
- [7] L. Montanaro, Durability of ceramic filters in the presence of some diesel soot oxidation additives, *Ceram. Int.* 25 (1999) 437–445.
- [8] T. Inui, T. Otowa, Catalytic combustion of benzene-soot captured on ceramic foam matrix, *Appl. Catal.* 14 (1985) 83–93.
- [9] P. Russo, P. Ciambelli, V. Palma, S. Vaccaro, Simultaneous filtration and catalytic oxidation of carbonaceous particulates, *Top. Catal.* 22 (1–2) (2003) 123–129.

- [10] F.A. Lammers, L.P.H. de Goeij, A numerical study of flash back of laminar premixed flames in ceramic-foam surface burners, *Combust. Flame* 133 (2003) 47–61.
- [11] S. Sharafat, et al., Micro-engineered first wall tungsten armor for high average power laser fusion energy systems, *JNM* 347 (3) (2005) 217–243.
- [12] S. Sharafat, N. Ghoniem, B. Williams, J. Babcock, Cellular foams: a potential innovative solid breeder material for fusion applications, *Fusion Sci. Technol.* 47 (4) (2005) 886–890.
- [13] A.J. Sherman, R.H. Tuffias, R.B. Kaplan, Refractory ceramic foams: a novel high-temperature structure, *Am. Ceram. Soc. Bull.* 70 (6) (1991) 1025–1029.
- [14] J.T. Richardson, Y. Peng, D. Remue, Properties of ceramic foam catalyst supports: pressure drop, *Appl. Catal. A: Gen.* 204 (2000) 19–32.
- [15] Ultramet Inc., Pacoima, CA 91331, USA.
- [16] T. Dummer, J.C. Lasalvia, G. Ravichandran, M.A. Meyers, Effect of strain rate on plastic flow and failure in polycrystalline tungsten, *Acta Mater.* 46 (17) (1998) 6267–6290.